1176 *Biochemistry* **2010,** *49,* 1176–1182
DOI: 10.1021/bi901772w

BIOCHEMISTRY
including biophysical chemistry & molecular biology
Article

Reaction Coordinate of Isopenicillin N Synthase: Oxidase versus Oxygenase Activity[†]

Christina D. Brown-Marshall, Adrienne R. Diebold, and Edward I. Solomon*

Department of Chemistry, Stanford University, Stanford, California 94305

Received October 14, 2009; Revised Manuscript Received January 13, 2010

ABSTRACT: Isopenicillin N synthase (IPNS) can have both oxidase and oxygenase activity depending on the substrate. For the native substrate, ACV, oxidase activity exists; however, for the substrate analogue ACOV, which lacks an amide nitrogen, IPNS exhibits oxygenase activity. The potential energy surfaces for the O−O bond elongation and cleavage were calculated for three different reactions: homolytic cleavage via traditional Fenton chemistry, heterolytic cleavage, and nucleophilic attack. These surfaces show that the hydroperoxide−ferrous intermediate, formed by O_2-activated H atom abstraction from the substrate, can exploit different reaction pathways and that interactions with the substrate govern the pathway. The hydrogen bonds from hydroperoxide to the amide nitrogen of ACV polarize the σ^* orbital of the peroxide toward the proximal oxygen, facilitating heterolytic cleavage. For the substrate analogue ACOV, this hydrogen bond is no longer present, leading to nucleophilic attack on the substrate intermediate C−S bond. After cleavage of the hydroperoxide, the two reaction pathways proceed with minimal barriers, resulting in the closure of the β-lactam ring for the oxidase activity (ACV) or formation of the thiocarboxylate for oxygenase activity (ACOV).

Isopenicillin N synthase is a mononuclear non-heme iron enzyme found in fungi and bacteria that catalyzes the formation of isopenicillin N, a bicyclic precursor of the β-lactam antibiotics, including the penicillins and cephalosporins (*1*, *2*). IPNS[1] binds tripeptide substrate δ-(L-α-aminoadipoyl)-L-cysteinyl-D-valine (ACV) and performs a four-electron oxidative double ring closure, fully reducing 1 equiv of O_2 to H_2O and closing the β-lactam and thiazolidine rings of isopenicillin N (*3*−*6*) (Scheme 1). This oxidase reactivity is unusual as most non-heme iron enzymes catalyze oxygenation reactions. Previous studies of the IPNS−ACV−$\{FeNO\}^7$ complex revealed that a major factor contributing to the oxidase reactivity of IPNS is the donation of charge from the ACV thiolate ligand, which renders the formation of the Fe^{III}−superoxide complex energetically favorable and drives the reaction only at the Fe center (*7*). This single-center, one-electron reaction allows IPNS to avoid the bridged binding of O_2 between the Fe^{II} and the substrate and/or cofactor required for its two-electron reduction, a reaction generally invoked for the non-heme Fe enzymes, that leads to oxygen insertion. The thiolate coordination of the IPNS−ACV substrate further activates the reactive Fe^{III}−superoxide complex of the enzyme through a configuration interaction with the bound superoxide π^* orbital which creates a frontier molecular orbital (FMO) with the correct orientation for abstraction of a H-atom from the ACV substrate (*7*).

Density functional theory (DFT) studies of the reaction coordinate of IPNS reveal that the Fe^{III}−superoxide FMO will conduct the H-atom abstraction from the cysteinyl β-carbon of ACV with a low barrier. Abstraction of a H-atom from ACV is accompanied by an additional transfer of an electron from the ACV substrate to yield an Fe^{II}−hydroperoxide complex and a double bond between the thiol sulfur and adjacent carbon of ACV (box in Scheme 2) (*8*−*11*). This IPNS−Fe^{II}−hydroperoxide complex is proposed to deprotonate either the amide nitrogen of ACV (*10*, *11*) or the iron-bound water (*9*) and cleave the O−O bond heterolytically, resulting in the formation of H_2O and an Fe^{IV}−oxo species. An S_N2-type reaction occurs between the lone pair on the ACV amide nitrogen and the carbon of the C−S double bond, leading to ring closure and formation of the β-lactam ring of isopenicillin N (center reaction in Scheme 1).

The heterolytic cleavage of the O−O bond of an Fe^{II}−hydroperoxide complex is unusual, as the Fe^{II}−hydroperoxide complex is generally thought to undergo Fenton chemistry to cleave the O−O bond homolytically, resulting in the production of a hydroxyl radical and an Fe^{III}−oxo(OH^-) species (*12*−*14*). Baldwin et al. have studied a series of ACV substrate analogues and have proposed mechanisms for their reactivity with dioxygen based upon crystal structures of the product complexes of these IPNS−Fe^{II}−analogue complexes after exposure to dioxygen (*15*−*19*). In one such analogue, ACOV, the amide nitrogen of the ACV valine is replaced with an oxygen atom as an ester, removing one of the proposed sources of the proton that could assist in O−O bond cleavage. Upon exposure to dioxygen, this analogue results in the hydroxylation of the cysteine carbon, effectively modifying the reactivity of IPNS from an oxidase to an oxygenase through a proposed nucleophilic attack of the Fe^{II}−hydroperoxide complex (*19*). In this study, DFT calculations calibrated by our experimental studies of the IPNS−ACV−$\{FeNO\}^7$ complex (*7*) were performed to explore how interactions of the substrate with the Fe^{II}−hydroperoxide moiety can avoid Fenton chemistry (homolytic cleavage) and modify the reactivity of this species, from heterolytic O−O bond cleavage to nucleophilic attack (Scheme 1). The exploration of factors governing reactivity (substrate direction of oxidase vs oxygenase

[†]This research was supported by National Institutes of Health Grant GM40392.

*To whom correspondence should be addressed. E-mail: edward.solomon@stanford.edu. Phone: (650) 723-4694. Fax: (650) 725-0259.

[1]Abbreviations: IPNS, isopenicillin N synthase; ACV, δ-(L-α-aminoadipoyl)-L-cysteinyl-D-valine; ACOV, δ-(L-α-aminoadipoyl)-L-cysteinyl-D-α-hydroxyisovaleryl ester.

 Published on Web 01/15/2010

Scheme 1: Four-Electron Oxidative Double Ring Closure of ACV To Form Isopenicillin N

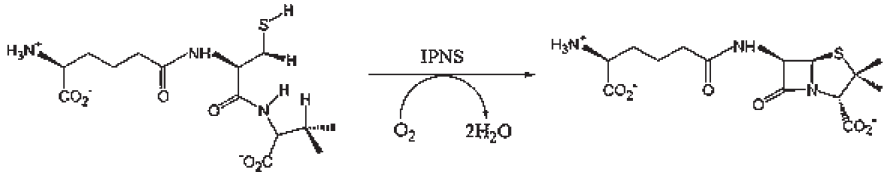

Scheme 2: Three Reaction Pathways of the Fe^{II}−Hydroperoxide Complex

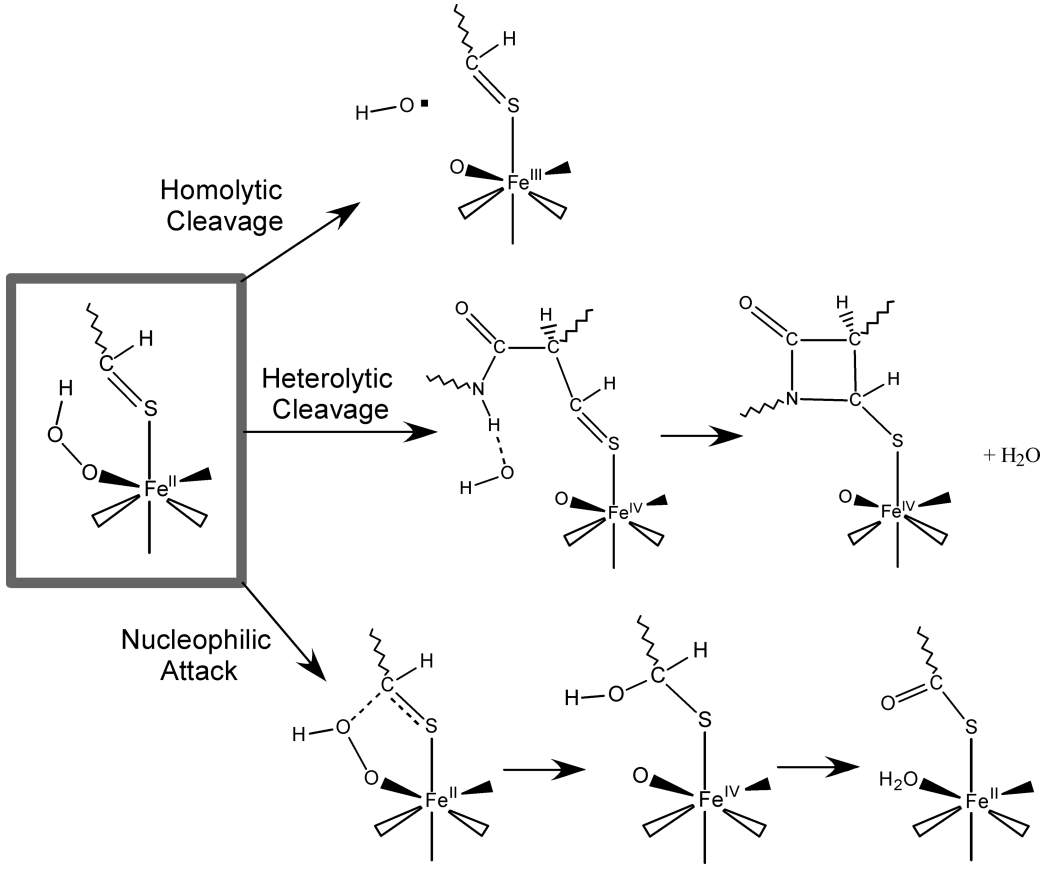

activity) adds a new facet of understanding to the body of knowledge of this important enzyme that has not been addressed in previous theoretical studies.

METHODS

The starting geometry for the Fe−IPNS−ACV−O_2 complex was taken from the crystal structure of the Fe−IPNS−ACV−NO complex from *Aspergillus nidulans* (*11*). Protein-derived ligands were truncated with methyl imidazoles modeling histidines and propionate modeling aspartate. The ACV substrate was truncated to remove the six-carbon aminoadipoyl chain but was otherwise left intact. The β-carbons of the protein ligands were frozen relative to each other to impose the constraints of the protein backbone. The cysteine nitrogen was also frozen relative to the β-carbons of the protein ligands to mimic hydrogen bonding to the substrate in the protein pocket.

All complexes were geometry-optimized using Gaussian 03 (*20*), with the spin-unrestricted BP86 functional (*21*, *22*) with 10% Hartree−Fock exchange under tight convergence criteria. This functional was previously calibrated for mononuclear non-heme iron $\{FeNO\}^7$ complexes (*23*). Geometry optimizations

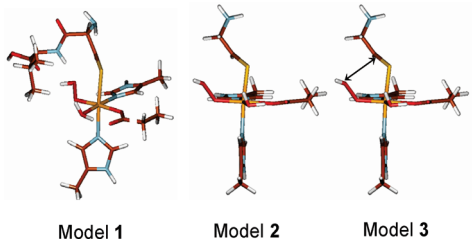

FIGURE 1: Models used to calculate three reaction pathways of the Fe^{II}−hydroperoxide complex. The arrow in model **3** indicates the extra constraint added to prohibit interaction of the distal oxygen with the carbon of the substrate.

were conducted using the Pople 6-311G* basis set on Fe, S, and the O_2 unit and the 6-31G* basis set on the remaining atoms. Single-point calculations were performed on the optimized structures to generate molecular orbitals using the functional and basis set described above. Orbital compositions were calculated using QMForge (*24*), and optimized structures and molecular orbitals were visualized using Molden version 4.1 (*25*). Frequencies and thermodynamic parameters were calculated using the split 6-311G*/6-31G* basis set. To best describe the effects of the interaction of the ACV sulfur with the

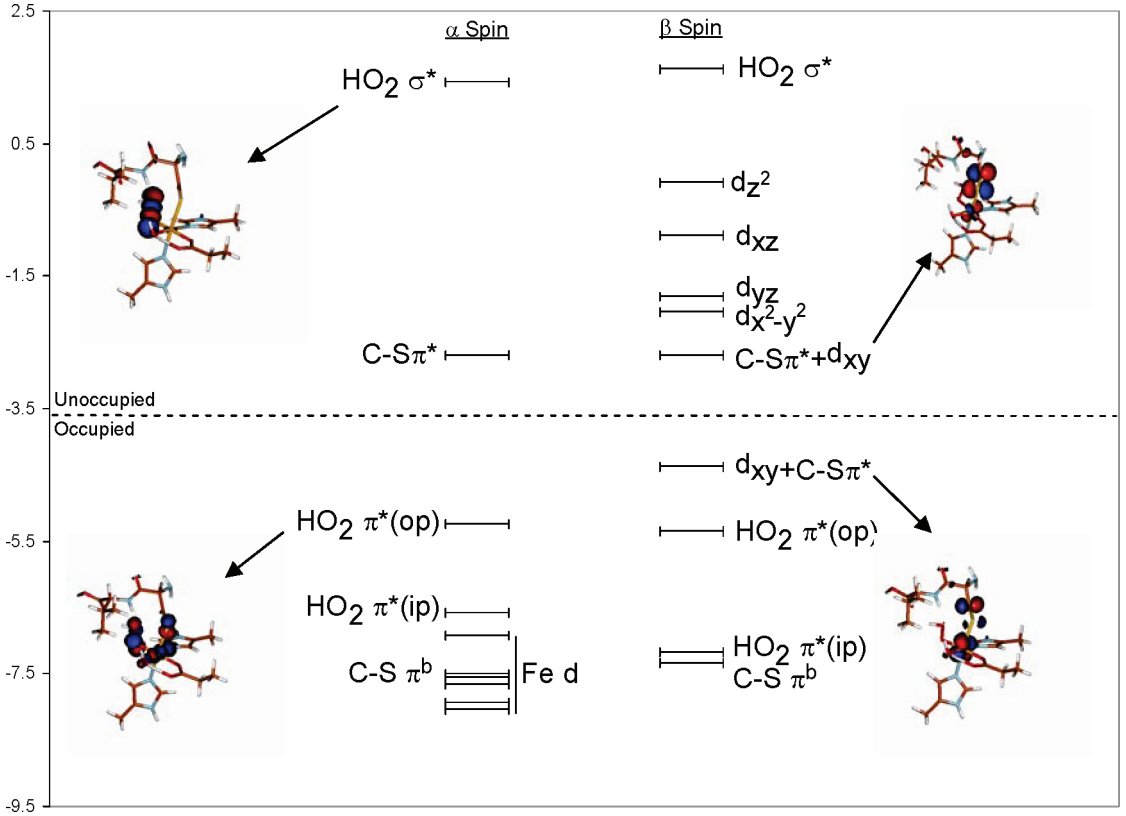

FIGURE 2: Molecular orbital diagram of the IPNS−ACV−Fe^{II}−hydroperoxide complex. Spin-unrestricted contours are given for representative molecular orbitals. Note the four unoccupied β d orbitals indicating Fe^{II} and the unoccupied α, β pair of the σ^* orbital of peroxide with the α, β unoccupied pair of C−S π^* orbitals of the substrate π bond. The observed d_{xy} character (24%) in the C−S π^* bond reflects backbonding.

Fe−IPNS models, single-point energies were calculated for the Fe−IPNS−ACV complexes using the 6-311+G(2d,p) basis set. Effects of solvation on the energy of the optimized structure were included using the polarized continuum model (PCM) (*26*) with a dielectric constant ε of 4.0 to model the protein environment. Cartesian coordinates for all models are given in the Supporting Information.

RESULTS

The potential energy surfaces (PES) for homolytic O−O bond cleavage, heterolytic O−O bond cleavage, and nucleophilic attack of three models of the IPNS active site were obtained as follows. The starting geometry for the Fe−IPNS−HO_2 complexes was taken from the previously optimized Fe−IPNS−ACV−O_2 structure (*7*) with subsequent ACV H-atom abstraction. After abstraction of a H-atom from the ACV carbon, the Fe^{II}−IPNS−ACV−HO_2 complex relaxes through reorientation of the hydroperoxide moiety to optimize hydrogen bonding interactions with the ACV amide and carboxylate residues (Figure 1, model **1**).[2] To model the nucleophilic attack by hydroperoxide seen for the ACOV substrate, we truncated the IPNS−Fe−ACV−HO_2 complex between the α-carbon and carbonyl carbon of the cysteine (Figure 1, model **2**), thus removing the amide nitrogen. Finally, this truncated ACOV model was used to explore the homolytic cleavage reaction via introduction of a constraint on the model to fix the distance between the distal peroxide oxygen atom and the carbon atom of the substrate, preventing the interaction of the distal oxygen with the ACOV carbon (Figure 1, model **3**).

For all three models that were studied, the electronic structure of the starting Fe^{II}−hydroperoxide complex is similar and is shown in Figure 2. Both the in-plane (ip) and out-of-plane (op) $2\pi^*$ orbitals of the hydroperoxide are fully occupied, and the unoccupied σ^* orbital of the hydroperoxide has come down in energy, in preparation for O−O bond cleavage (*27*). As previously described (*9*), the Fe d_{xy} orbital in the β-manifold is occupied, and a double bond has formed between the cysteine carbon and sulfur atoms, evidenced by the unoccupied C−S π^* orbital in both the α- and β-manifolds. At the optimized O−O bond length, there is a mixing of the occupied β Fe d_{xy} orbital and the C−S π^* orbital, which is indicative of backbonding of the occupied Fe^{II} d orbital into the C−S π^* double bond. As the O−O bond is elongated, this backbonding is alleviated, localizing the electron on the Fe and allowing the occupied β Fe d_{xy} orbital to rotate to interact with the descending hydroperoxide σ^* orbital (Figure S1 of the Supporting Information).

Starting with the optimized Fe^{II}−hydroperoxide structures, we explored the PES of each model by optimizing each structure by incrementally increasing the O−O bond distance until the O−O bond was fully cleaved. Optimized geometries for the O−O elongation along the PES's of **1**, **2**, and **3** are shown in Figure 3, and key computational results are summarized in Table S1 of the Supporting Information. The PES of **3** corresponds to the expected Fenton chemistry with homolytic cleavage of the O−O bond. This homolytic cleavage is accomplished by transfer of one β-electron from the Fe d_{xy} orbital to the O−O σ^* orbital (Figure 4, left), resulting in the formation of an Fe^{III}−oxo complex and a hydroxyl radical. This is evidenced by the

[2]The reorientation of the hydroperoxide was accomplished through contraction of the distance between the ACV amide nitrogen and cysteinyl carbon to approximately 2.8 Å.

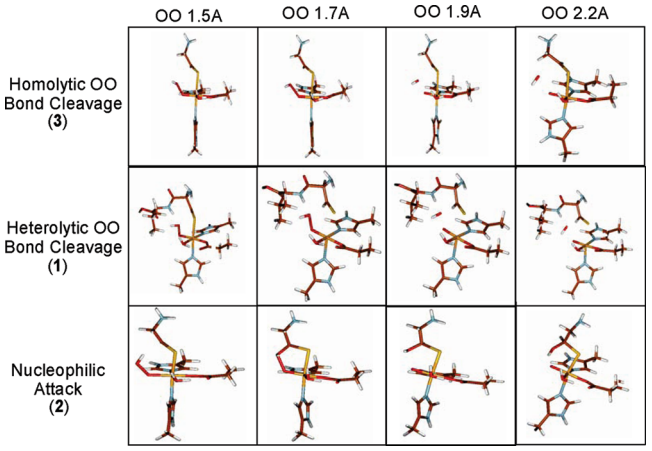

FIGURE 3: Geometric structures of IPNS−Fe^{II}−hydroperoxide complexes with O−O bond elongation. The three models undergo homolytic cleavage (top, **3**), heterolytic O−O bond cleavage (middle, **1**), and nucleophilic attack by the peroxide (bottom, **2**).

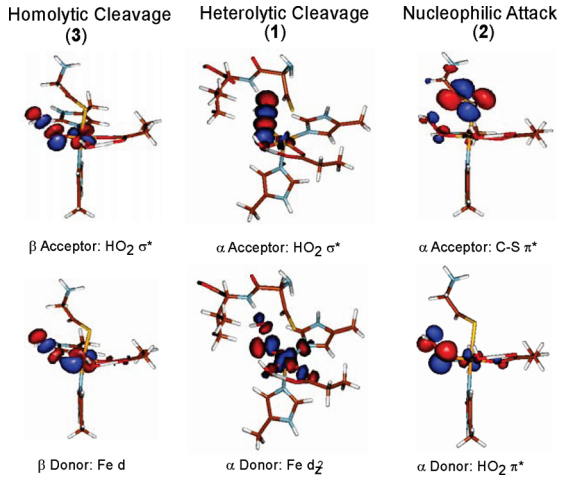

FIGURE 4: Donor and acceptor orbitals for homolytic cleavage, heterolytic cleavage, and nucleophilic attack. In the homolytic cleavage reaction, one β-electron is transferred from the Fe d orbital to the hydroperoxide σ* orbital. Heterolytic cleavage and nucleophilic attack involve the transfer of an α, β electron pair. For the sake of clarity, only the α-donor and -acceptor orbitals of these electron pairs are shown.

accumulation of negative spin density on the distal oxygen [−0.48 at a O−O bond distance of 2.20 Å (see Table S1 of the Supporting Information)]. The PES of **1** (Figure 3, middle) proceeds as a heterolytic cleavage of the O−O bond, with one electron in each spin manifold transferred from the β Fe d_{xy} orbital and the α Fe d_{z^2} orbital into the O−O σ* orbital (Figure 4, middle). This produces an Fe^{IV}−oxo complex and hydroxide, which remains within hydrogen bonding distance of the amide of the ACV valine (Figure 3, middle right). The PES of model **2** involves a nucleophilic attack of the hydroperoxide moiety at the ACOV carbon followed by heterolytic O−O bond cleavage (Figure 3, bottom). Nucleophilic attack is accomplished by the transfer of an electron pair from the peroxide π* out-of-plane orbital to the C−S π* orbital (Figure 4, right), followed by two-electron transfer from the Fe^{II} to the O−O σ* orbital to give an Fe^{IV}−oxo complex with a hydroxylated substrate carbon.

These calculated model reactions demonstrate that the same Fe^{II}−hydroperoxide unit can undergo different reaction modes. The factors that govern the choice of reaction pathways were

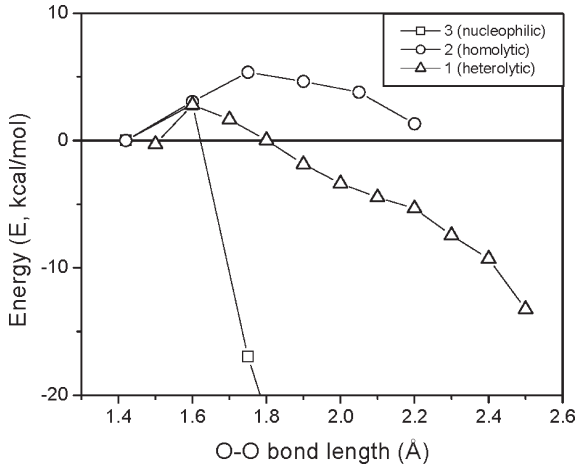

FIGURE 5: Energetics of O−O bond cleavage. The relative electronic energies are plotted for homolytic cleavage (**3**, circles), heterolytic cleavage (**1**, triangles), and nucleophilic attack (**2**, squares) models as the O−O bond is elongated. Note that the nucleophilic attack model is valid for only O−O bond cleavage in ACOV and that for the ACV substrate, an additional barrier to break the amide−peroxide hydrogen bond is present.

evaluated further. Table S1 of the Supporting Information shows that at short distances, models **1** (heterolytic) and **3** (homolytic) exhibit similar electronic structures up to 1.9 Å for the transfer of the first electron from Fe^{II} to the hydroperoxide σ* orbital. A plot of the energies along the reaction coordinate for models **1** (heterolytic) and **3** (homolytic) (Figure 5) shows an initial stabilization of this electron transfer, and this stabilization is expected to be similar for the second electron in the heterolytic O−O bond cleavage pathway as opposed to the homolytic pathway. In a comparison of the structures, the distal oxygen of the heterolytically cleaving **1** is within hydrogen bonding distance of the amide proton of the ACV valine, while the distal oxygen of the homolytic coordinate **3** has no such interaction. This hydrogen bond in **1** stabilizes the transfer of both electrons to the distal oxygen.

Importantly, **1** has an unoccupied σ* orbital that is polarized toward the proximal oxygen (Op, Figure 6, left), while the σ* orbital of **3** is polarized toward the distal oxygen (Od, Figure 6, middle). When the σ* orbital is polarized toward the proximal oxygen, its bonding σ counterpart is polarized toward the distal oxygen. As this peroxide σ orbital is fully occupied, this polarization will lead to an electron pair being transferred to the distal oxygen upon O−O bond cleavage and, thus, the heterolytic cleavage of the O−O bond. Polarization of the σ* orbital toward the distal oxygen allows only for the transfer of a single electron to the distal oxygen and results in homolytic cleavage. The hydrogen bonding interaction of **1** can be modeled via addition of an equivalent point dipole to **3**, which reverses the polarization of the σ* orbital (Figure 6, right). Elongation of the O−O bond in the presence of a point dipole also leads to heterolytic cleavage (Table S2 of the Supporting Information). Therefore, it is the interaction of the dipole of the amide N−H bond with the distal oxygen in **1** that directs the ACV complex toward heterolytic cleavage of the O−O bond.

In a comparison of the nucleophilic attack relative to the heterolytic O−O bond cleavage (**2** vs **1**), both of these pathways proceed with similarly small reaction barriers (Figure 5). From a more detailed transition state analysis of model **1**, the $\Delta G^{\ddagger}$ is 4.1 kcal/mol (the coordinates are given in Table S5 of the

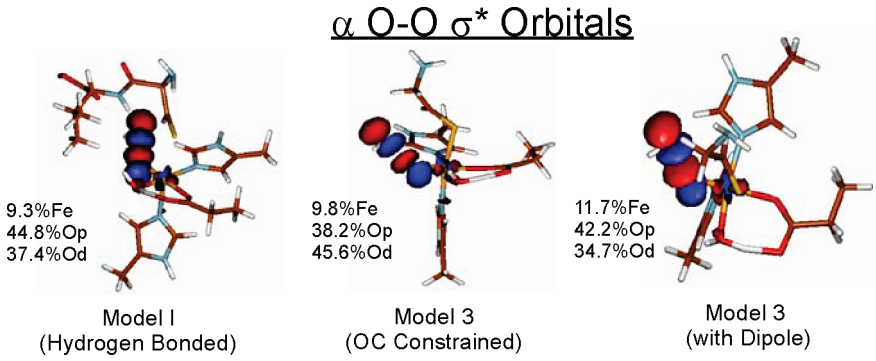

FIGURE 6: α-Hydroperoxide σ^* orbitals. This orbital polarizes toward the proximal oxygen in model **1**, directing the reaction to heterolytic O−O bond cleavage, and toward the distal oxygen in model **3**, directing its reaction to homolytic O−O bond cleavage. By modeling the dipole interaction of the ACV amide N−H bond, the polarization of the σ^* bond in model **3** is reversed.

Scheme 3: Rotation of the Peroxide for Nucleophilic Attack

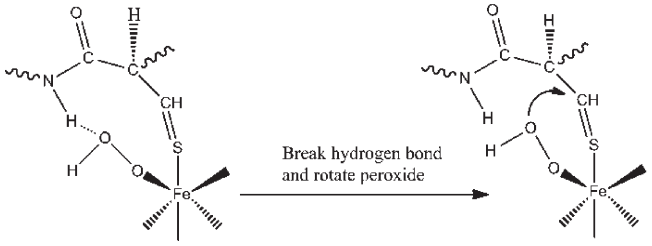

Supporting Information; the transition state occurs at an O−O bond length of approximately 1.6 Å). For **1** to undergo a nucleophilic attack, the hydrogen bond between the distal oxygen and the amide proton would have to be broken to allow the peroxide to rotate to the proper orientation (Scheme 3).

The strength of the hydrogen bonding interaction that must be broken for the hydroperoxide to undergo this rotation is calculated to be 5.6 kcal/mol, which is already larger than the barrier for heterolytic cleavage (Figure 5). This hydrogen bonding interaction with the amide proton in **1** would thus bias the reaction of the Fe^{II}−hydroperoxide complex toward heterolytic cleavage over nucleophilic attack. In this way, the hydrogen bonding interaction of the Fe^{II}−hydroperoxide complex helps distinguish between reactions possible for the IPNS−Fe^{II}−hydroperoxide−ACV intermediate. As the iron-bound water [the alternate proposed source for the proton in the reaction with ACV (*9*)] would be present in both the IPNS−Fe^{II}−hydroperoxide−ACV and IPNS−Fe^{II}−hydroperoxide−ACOV complexes, hydrogen bonding to the water would direct both complexes toward heterolytic cleavage of the O−O bond. Thus, the observed nucleophilic reactivity of the ACOV complex argues strongly against the coordinated water being the source of the proton in either reaction.

The coordinates were extended beyond O−O bond cleavage to complete the reaction cycle for the different substrates. For **1**, the hydroxide produced upon O−O bond cleavage is within hydrogen bonding distance of the amide proton of the ACV valine and can abstract this proton with a negligible barrier (< 1 kcal/mol) compared to that of the previous intermediate. This leaves a lone pair of electrons on the valine amide with appropriate overlap for an S_N2-type reaction with the C−S π^* orbital to close the β-lactam ring of isopenicillin N (Figure 7). The orientation of the lone pair on the ACV amide is mechanistically significant; thus, the ACV amide must be deprotonated before β-lactam ring closure. This reaction pathway is similar to that described in ref *10*. For **2**, the transfer of two protons, one from the hydroxyl group and one from the hydroxylated carbon of ACOV, to the Fe−oxo intermediate would lead to the Fe−IPNS−thiocarboxylate structure observed (*19*) for the oxygen-exposed Fe−IPNS−ACOV complex (Scheme 2, bottom).

DISCUSSION

In the first stage of the reaction of the IPNS−Fe^{II}−ACV complex with dioxygen, the ACV thiolate bond activates the one-electron reduction of dioxygen to form an Fe^{III}−superoxide complex with good FMO overlap for abstraction of a H-atom from the substrate (*7*). This is atypical for most mononuclear non-heme Fe enzymes as seen in, for example, the α-ketoglutarate-dependent and extradiol dioxygenases, in which the unfavorable one-electron reduction of O_2 is circumvented by adoption of a bridged binding mode allowing $2e^-$ reduction that results in oxygenase activity. This mechanism of a one-electron reduction of O_2 avoids its bridged binding to substrate and opens up a pathway for oxidase activity in IPNS not energetically available for other mononuclear non-heme Fe enzymes.

The initial H-atom abstraction in IPNS is calculated to produce an Fe^{II}−hydroperoxide complex that can undergo a variety of reaction channels, dependent upon its interaction with the substrate. While Fe^{II}−hydroperoxide species are generally thought to undergo Fenton chemistry (i.e., homolytic O−O bond cleavage in solution), the experimental evidence from reactions of IPNS−Fe^{II}−ACV and analogue complexes suggests that an Fe^{II}−hydroperoxide species can follow alternative reaction pathways, including heterolytic O−O bond cleavage and nucleophilic attack by the peroxide at a substrate double bond. DFT calculations on three IPNS−Fe^{II}−HO_2 models show that all three of the reaction pathways mentioned above are energetically accessible.

A fourth reaction pathway, not invoked in previous IPNS mechanisms but proposed for hydroxyethylphosphonate dioxygenase (HEPD), involves attack via the proximal oxygen of the hydroperoxide (with respect to the Fe center). This reaction is different from HEPD in that, for IPNS, it would involve the nucleophilic attack by the hydroperoxide but in HEPD a hydroperoxylation is invoked (*28*). To evaluate this pathway, the $C\cdots O_p$ reaction coordinate was examined. Starting from the optimized Fe^{II}−hydroperoxide structure (Figure 1, model **2**), the attack by the proximal oxygen occurs with a barrier of 2−3 kcal/mol, comparable to that observed in Figure 4 for the nucleophilic attack by the distal oxygen. Upon formation of the $C-O_p$ bond, the C−S thioaldehyde is reduced while the Fe center

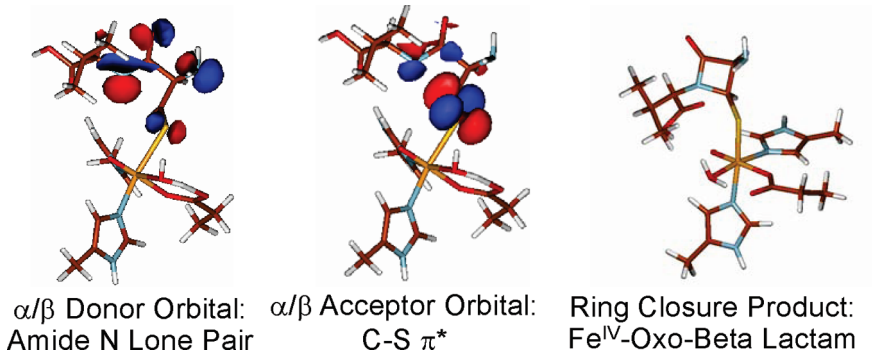

FIGURE 7: Donor and acceptor orbitals and product for β-lactam ring closure. Deprotonation of the ACV amide leaves a lone pair on the amide N with the correct orientation for SN_2 nucleophilic attack at the C−S double bond.

Scheme 4: Nucleophilic Attack by the Distal and Proximal Oxygen of the Hydroperoxide

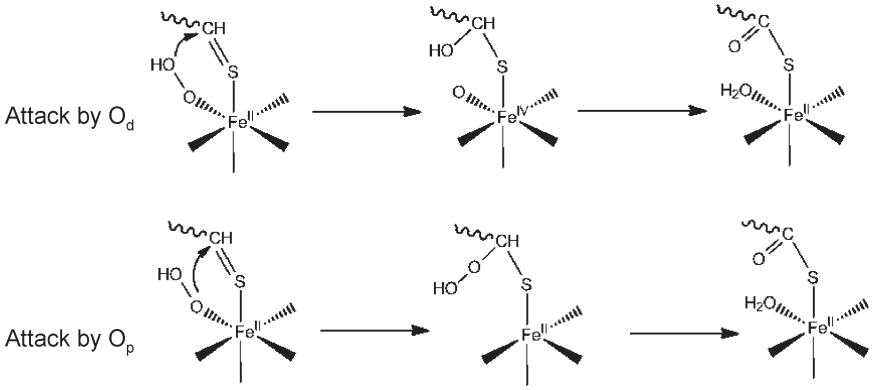

remains Fe^{II} (Scheme 4, bottom). This intermediate is lower in energy than the starting structure by ~21 kcal/mol [compared to −67 kcal/mol for the Fe^{IV}−oxo intermediate from the nucleophilic attack by the distal oxygen (Scheme 4, top)]. From this intermediate, the O−O bond can be cleaved heterolytically and a proton lost from the C center to give the crystallographically observed thiocarboxylate intermediate. Although along a different reaction coordinate and with less driving force, attack by the proximal oxygen appears to be an additional, viable pathway that will lead to the product observed via crystallography.

The DFT calculations show that the interactions of the substrate with the Fe^{II}−hydroperoxide moiety can determine its reactivity. For the ACV substrate, hydrogen bonding interactions with the amide hydrogen polarize the peroxide σ^* orbital to make the heterolytic cleavage of the O−O bond energetically favorable. In the absence of this hydrogen bonding interaction, nucleophilic attack of either the distal or proximal O of the hydroperoxide at the carbon of the ACV C−S double bond occurs, leading to the substrate hydroxylation observed experimentally for ACOV. In this way, the hydrogen bonding interaction with the ACV substrate directs the Fe^{II}−hydroperoxide moiety to heterolytic cleavage and enables the unusual oxidase activity of this enzyme.

ACKNOWLEDGMENT

We thank Dr. Marcus Lundberg for insightful discussions.

SUPPORTING INFORMATION AVAILABLE

Full reference for ref *20*, alleviation of backbonding with O−O bond elongation, bond lengths and spin densities for elongation of the O−O bond, and Cartesian coordinates for selected structures. This material is available free of charge via the Internet at http://pubs.acs.org.

REFERENCES

1. Baldwin, J. E., Adlington, R. M., Moroney, S. E., Field, L. D., and Ting, H. H. (1984) Stepwise Ring-Closure in Penicillin Biosynthesis: Initial β-Lactam Formation. *J. Chem. Soc., Chem. Commun.*, 984–986.
2. Baldwin, J. E., and Abraham, E. (1988) The Biosynthesis of Penicillins and Cephalosporins. *Nat. Prod. Rep. 5*, 129–145.
3. Chen, P., and Solomon, E. I. (2004) Oxygen activation by the noncoupled binuclear copper site in peptidylglycine α-hydroxylating monooxygenase. Reaction mechanism and role of the noncoupled nature of the active site. *J. Am. Chem. Soc. 126*, 4991–5000.
4. Orville, A. M., Chen, V. J., Kriauciunas, A., Harpel, M. R., Fox, B. G., Munck, E., and Lipscomb, J. D. (1992) Thiolate Ligation of the Active-Site Fe^{2+} of Isopenicillin-N Synthase Derives from Substrate Rather Than Endogenous Cysteine: Spectroscopic Studies of Site-Specific Cys → Ser Mutated Enzymes. *Biochemistry 31*, 4602–4612.
5. Randall, C. R., Zang, Y., True, A. E., Que, L., Charnock, J. M., Garner, C. D., Fujishima, Y., Schofield, C. J., and Baldwin, J. E. (1993) X-ray-Absorption Studies of the Ferrous Active-Site of Isopenicillin N-Synthase and Related Model Complexes. *Biochemistry 32*, 6664–6673.
6. Scott, R. A., Wang, S. K., Eidsness, M. K., Kriauciunas, A., Frolik, C. A., and Chen, V. J. (1992) X-ray Absorption Spectroscopic Studies of the High-Spin Iron(Ii) Active-Site of Isopenicillin-N Synthase: Evidence for Fe-S Interaction in the Enzyme Substrate Complex. *Biochemistry 31*, 4596–4601.
7. Brown, C. D., Neidig, M. L., Neibergall, M. B., Lipscomb, J. D., and Solomon, E. I. (2007) VTVH-MCD and DFT studies of thiolate bonding to $\{FeNO\}^7/\{FeO_2\}^8$ complexes of isopenicillin N synthase: Substrate determination of oxidase versus oxygenase activity in nonheme Fe enzymes. *J. Am. Chem. Soc. 129*, 7427–7438.
8. Lundberg, M., and Morokuma, K. (2007) Protein environment facilitates O-2 binding in non-heme iron enzyme. An insight from ONIOM calculations on isopenicillin N synthase (IPNS). *J. Phys. Chem. B 111*, 9380–9389.

9. Lundberg, M., Siegbahn, P. E. M., and Morokuma, K. (2008) The mechanism for isopenicillin N synthase from density-functional modeling highlights the similarities with other enzymes in the 2-his-1-carboxylate family. *Biochemistry 47*, 1031–1042.
10. Lundberg, M., Kawatsu, T., Vreven, T., Frisch, M. J., and Morokuma, K. (2009) Transition States in a Protein Environment: ONIOM QM:MM Modeling of Isopenicillin N Synthesis. *J. Chem. Theory Comput. 5*, 222–234.
11. Roach, P. L., Clifton, I. J., Hensgens, C. M. H., Shibata, N., Schofield, C. J., Hajdu, J., and Baldwin, J. E. (1997) Structure of isopenicillin N synthase complexed with substrate and the mechanism of penicillin formation. *Nature 387*, 827–830.
12. Haber, F., and Weiss, J. (1934) The Catalytic Decomposition of Hydrogen Peroxide by Iron Salts. *Proc. R. Soc. London, Ser. A 147*, 332–351.
13. MacFaul, P. A., Wayner, D. D. M., and Ingold, K. U. (1998) A radical account of "oxygenated Fenton chemistry". *Acc. Chem. Res. 31*, 159–162.
14. Walling, C. (1975) Fentons Reagent Revisited. *Acc. Chem. Res. 8*, 125–131.
15. Ge, W., Clifton, I. J., Stok, J. E., Adlington, R. M., Baldwin, J. E., and Rutledge, P. J. (2008) Isopenicillin N synthase mediates thiolate oxidation to sulfenate in a depsipeptide substrate analogue: Implications for oxygen binding and a link to nitrile hydratase? *J. Am. Chem. Soc. 130*, 10096–10102.
16. Long, A. J., Clifton, I. J., Roach, P. L., Baldwin, J. E., Schofield, C. J., and Rutledge, P. J. (2003) Structural studies on the reaction of isopenicillin N synthase with the substrate analogue δ-(L-α-aminoadipoyl)-L-cysteinyl-D-α-aminobutyrate. *Biochem. J. 372*, 687–693.
17. Long, A. J., Clifton, I. J., Roach, P. L., Baldwin, J. E., Rutledge, P. J., and Schofield, C. J. (2005) Structural studies on the reaction of isopenicillin N synthase with the truncated substrate analogues δ-(L-α-aminoadipoyl)-L-cysteinyl-glycine and δ-(L-α-aminoadipoyl)-L-cysteinyl-D-alanine. *Biochemistry 44*, 6619–6628.
18. Howard-Jones, A. R., Rutledge, P. J., Clifton, I. J., Adlington, R. M., and Baldwin, J. E. (2005) Unique binding of a non-natural L,L,L-substrate by isopenicillin N synthase. *Biochem. Biophys. Res. Commun. 336*, 702–708.
19. Ogle, J. M., Clifton, I. J., Rutledge, P. J., Elkins, J. M., Burzlaff, N. I., Adlington, R. M., Roach, P. L., and Baldwin, J. E. (2001) Alternative oxidation by isopenicillin N synthase observed by X-ray diffraction. *Chem. Biol. 8*, 1231–1237.
20. Frisch, M. J., et al. (2007) Gaussian03, revision E.01, Gaussian, Inc., Wallingford, CT.
21. Perdew, J. P. (1986) Density-Functional Approximation for the Correlation-Energy of the Inhomogeneous Electron-Gas. *Phys. Rev. B 33*, 8822–8824.
22. Becke, A. D. (1988) Density-Functional Exchange-Energy Approximation with Correct Asymptotic-Behavior. *Phys. Rev. A 38*, 3098–3100.
23. Schenk, G., Pau, M. Y. M., and Solomon, E. I. (2004) Comparison between the geometric and electronic structures and reactivities of $\{FeNO\}^7$ and $\{FeO_2\}^8$ complexes: A density functional theory study. *J. Am. Chem. Soc. 126*, 505–515.
24. Tenderholt, A. L. (2007) QMForge, version 2.1, Stanford University, Stanford, CA.
25. Schaftenaar, G., and Noordik, J. H. (2000) Molden: A pre- and post-processing program for molecular and electronic structures. *J. Comput.-Aided Mol. Des. 14*, 123–134.
26. Cramer, C. J., and Truhlar, D. G. (1999) Implicit solvation models: Equilibria, structure, spectra, and dynamics. *Chem. Rev. 99*, 2161–2200.
27. Neese, F., Zaleski, J. M., Zaleski, K. L., and Solomon, E. I. (2000) Electronic structure of activated bleomycin: Oxygen intermediates in heme versus non-heme iron. *J. Am. Chem. Soc. 122*, 11703–11724.
28. Whifteck, J. T., Cicchillo, R. M., and van der Donk, W. A. (2009) Hydroperoxylation by Hydroxyethylphosphonate Dioxygenase. *J. Am. Chem. Soc. 131*, 16225–16232.